Simultaneous removal of bacteria and volatile organic compounds on Cu2O-NPs decorated TiO2 nanotubes: Competition effect and kinetic studies

M Abidi, A Hajjaji, A. Bouzaza, K. Trablesi, H Makhlouf, S. Rtimi, A.A. Assadi, B. Bessais

Simultaneous removal of bacteria and volatile organic compounds on Cu_2O-NPs decorated TiO_2 nanotubes: competition effect and kinetic studies

M. Abidi[1,2,3], A Hajjaji[1], A. Bouzaza[2], K Trablesi[1], H. Makhlouf[4], S. Rtimi[5], A.A. Assadi[2]*, B. Bessais[1]

[1] *Centre de Recherches et des Technologies de l'Energie, Technopole de Borj-Cédria, BP 95, 2050 Hammam-Lif, Tunisia*
[2]*Univ Rennes, ENSCR, ISCR (Institut des Sciences Chimiques de Rennes), UMR 6226, F-35000 Rennes, France*
[3]*Universite de Tunis El Manar, BP 94, Rommana, 1068 Tunis, Tunisia*
[4]*Laboratory of Nanomaterials and Systems for Renewable Energy, Centre de Recherches et des Technologies de l'Energie, Technopole de Borj-Cédria, BP 95, 2050 Hammam-Lif, Tunisia*
[5]*Ecole Polytechnique Fédérale de Lausanne (EPFL), CH-1015, Lausanne, Switzerland*

□Corresponding authors: E-mail address: aymen.assadi@ensc-rennes.fr (A.A. Assadi)

Graphical abstract:

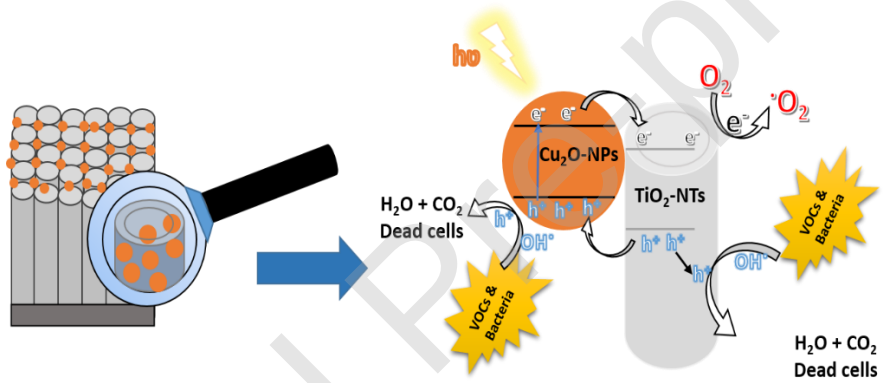

Highlights:

- Preparation and characterization of Cu_2O-NPs decorated TiO_2 nanotubes.
- Cu_2O-NPs/TiO_2-NTs has greatest photocatalytic performance under UV-Visible light irradiation.
- Simultaneous removal of *E. coli* and Butane-2, 3-Dione (BUT) was studied.
- Mechanism of the photocatalytic activities is suggested.

Abstract:

In this work, we study the effect of decorating TiO_2 nanotubes (TiO_2-NTs) with Cu_2O nanoparticles (Cu_2O-NPs) on photocatalytic degradation of volatile organic compounds (VOCs) and on bacterial disinfection. The Cu_2O-NPs were loaded on the TiO_2-NTs by the electrodeposition method. The butane-2, 3-dione (BUT) was used as a target VOC-pollutant of food industry due its adverse environmental impact (high toxicity and confirmed carcinogenicity). The achieved Cu_2O-NPs/TiO_2-NTs nanocomposites were characterized using X-ray diffraction (XRD), photoluminescence (PL), diffuse reflectance spectroscopy (UV-Vis) and scanning (SEM) and transmission (TEM) electron microscopy. In order to investigate the photocatalytic and antibacterial behavior of the Cu_2O-NPs/TiO_2-NTs, simultaneous removal of *Escherichia coli* (*E. coli*) and butane-2, 3-dione (BUT) were tested with the optimized catalyst. We observed a bacterial inactivation rate of 98% and a concomitant 99.7% VOC removal within 60 min and 25 min of visible light irradiation, respectively.

Keywords: Cu_2O-NPs /TiO_2 nanotubes, batch reactor, Simultaneous removal, Bacterial inactivation, kinetic modelling

1-Introduction

Nowadays air pollution is not limited to the outside; it also includes indoor spaces, in which we spend about 90% of our time. Air quality is an important risk factor for human health [1], so the control and purity of the breathed air is of prime importance today. Indoor air is characterized by a set of physical, chemical or biological pollutants of different origins [2-4]. For this reason, technologies that have the ability to purify air from organic contaminants with efficient and inexpensive processes became the objective of many research groups [5, 6]. Thus, several remediation techniques were used to reduce this kind of pollutants using photocatalysts [7, 8], non-thermal plasma [9,10], catalytic ozonation [11]. Scientific studies on photocatalysis started about four decades ago and showed that photocatalysis can be an interesting technique for environmental remediation [7, 8, 12]. It is based on the activation of semiconductors by light irradiation making it possible to form active chemical species such as hydroxyl radicals (OH°) leading to the degradation of pollutants [7]. Metal oxide semiconductors received much attention due to their important applications in catalysis, optoelectronics, hydrogen generation and solar cells [13-19]. Titanium dioxide (TiO_2) is one of the most studied photocatalyst due to its non-toxicity, low cost, high chemical stability and environmental friendliness [13]. Many nano-forms of TiO_2 such as nano-rods [14],

nanowires, nanoparticles [21] and nanotubes [22-25] have been widely studied for environmental purpose. TiO_2 NTs having different structures and sizes may be achieved by different synthetic routes such as template assisted technique, electrochemical anodization, hydrothermal and solvothermal methods, and sol-gel deposition [17, 26-28]. TiO_2 nanotubular layers possess excellent photocatalytic properties that are significantly enhanced compared to nanoparticulate layers [25]. Large area (~50 cm^2) of TiO_2 nanotube layer may be achieved for photocatalysis in a gaseous phase [29]. The disadvantage of TiO_2 materials is its wide band gap (3.2 eV in anatase phase), which allows it to absorb only ultraviolet radiation, thus limiting its use under sunlight. To overcome this limitation, numerous attempts have been made to sensitize TiO_2 NTs via surface modification: metal or non-metal doping [30, 31], and coupling with other narrow band gap semiconductors [32 - 34]. The surface or doping modifications introduced in TiO_2 could avoid the recombination of the photogenerated electron-hole pairs and then widen the absorption spectral range of the catalyst in the visible [18, 20-22, 34-36]. It has been shown that Ag- V- and Fe-doped TiO_2 achieved by various routes are very efficient in the oxidation of VOCs (butyl acetate, hexane or gaseous toluene) [37, 38]. It has been shown that self-organized TiO_2 nanotube layers can be used for photo-induced cancer cell killing [39]. The same studies reported enhanced photocatalytic oxidation and indoor photocatalytic disinfection of gaseous toluene and *Escherichia coli* (*E. coli*) [40] than un-doped TiO_2/PU. It was also proven that coupling TiO_2 with low band-gap semiconductor heterostructures is very efficient in sunlight-driven Photocatalysis [41]. According to relative energy band positions between TiO_2 and visible-light-absorbing semiconductors, we can distinguish three different types of heterojunction (Fig. 1).

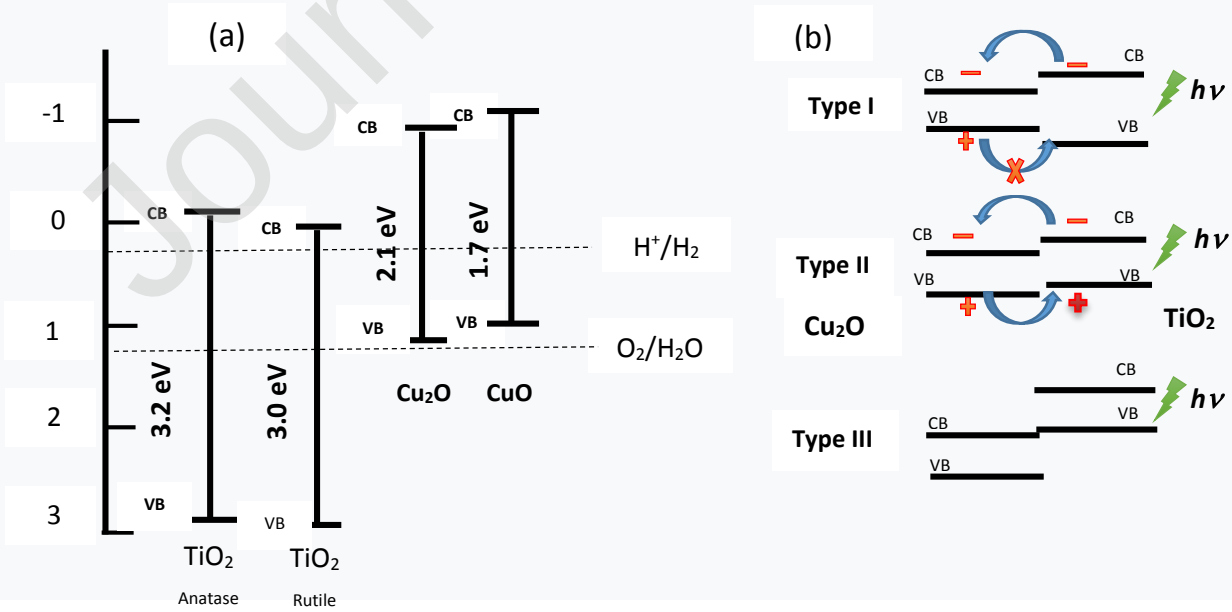

Figure 1: (a) Band gap energies and band positions of Titania (anatase and rutile) and copper oxides-values of band positions were taken from the reference. (b) Types of heterojunction system of coupled semiconductors. CB, VB, and NHE are the abbreviations of conduction band, valance band, and normal hydrogen electrode, respectively. ***Reprinted with permission from*** **[42]**.

In Type-I heterojunction, the conduction band (CB) level of the sensitizer is positioned more negatively than that of TiO_2, whereas in Type-II system its valence band (VB) level is more positive than that of TiO_2. Cu_2O is a semiconductor that can satisfy this Type-II condition (Fig. 1-a). In Type-III system, the sensitizer energy level is located between the CB and VB of TiO_2. It was shown that type II has noticeably higher photocatalytic efficiency than type I, whereas type III did not show any appreciable improvement. Remarkably high visible-light photocatalytic activity of Type-II heterojunction structures could be explained by inter-semiconductor hole-transfer mechanism between the VB of sensitizer and that of TiO_2. Cuprous oxide (Cu_2O) is a p-type semiconductor material having a direct optical band gap energy in the 1.9 -2.3 eV range that can form a type II system with TiO_2 (Figure 1-b) [42].
The variation of the Cu_2O band gap energy (1.9 -2.3 eV) depends on the synthesis method [43-46]. Cu_2O has been applied in many fields such as water splitting, gas sensor, solar cells, photocatalytic process etc. [44 - 47]. It has been shown that Cu_2O/TiO_2 type heterojunction enhances sunlight electrocatalytic activity [46]. Indeed, the response of Cu_2O under visible light and that of TiO_2 under UV light allow the use of sunlight. On the other hand, the photogenerated electrons at conduction band (CB) of Cu_2O surface can be easily transferred to the CB of TiO_2 (Fig. 1), while holes can be transferred from the valence band (VB) of TiO_2 to the VB of Cu_2O, since both Cu_2O bands (CB and VB) are more negative than those of TiO_2 [42]. Tran et al. [46] used Cu_2O nanoparticles to modify TiO_2-NTs by the photoreduction method using a low-power UV lamp. As results, Cu_2O - modified samples showed a photo-degradation rate of methylene blue increased two to three time compared to pure NTs. The enhanced efficiency was attributed to the Cu_2O narrow band gap and the defect states produced by the oxygen vacancies in the proximity of heterojunctions. The band levels (conduction and valence bands) of both semiconductors play the most important role in the separation of the photogenerated electron-hole pairs, which reduce the recombination rate via the internal electric field across the Cu_2O/TiO_2-NTs interface [47].
In this work, we prepared and characterized Cu_2O/TiO_2-NTs nanocomposites by depositing Cu_2O nanoparticles into entire TiO_2 NTs structures using the electrodeposition method [48]. The photocatalytic performances of the Cu_2O/TiO_2-NTs were evaluated under UV-Visible light for separate and simultaneous removal of *E. coli* and volatile organic compounds

(VOC). To our knowledge, there is no study on the catalytic activity of Cu_2O/TiO_2-NTs for the elimination of double pollution (bacteria and VOC) in indoor air.

2- Experimental

2.1. Preparation of TiO_2-NTs and Cu_2O/TiO_2-NTs photo-electrodes

The TiO_2-NTs were synthesized by the electrochemical anodization method [48]. In summary, prior to anodization, titanium foils (99%) were polished with grain-size abrasive paper ranging from 320 to 2000 µm, and then ultrasonically cleaned with acetone, ethanol, and bi-distilled water before air-drying. The anodization process was unrolled in a two-electrode electrochemical cell with the titanium foil used as the anode and a platinum wire as the cathode. The anodization process was carried out under continuous stirring during 2 hours at room temperature and at a constant potential of 60 V. The electrolyte consists of an electrolytic solution containing 2 vol% of ethylene glycol (in ultrapure water) and [NH4F] of 0.07 mol/L.The as-prepared TiO_2 NTs were annealed for 3 hours at 400 °C (temperature increase rate: 5 °C min^{-1}) after being rinsed with water and air dried for subsequent electrochemical deposition. The electroplating of Cu_2O nanoparticles on TiO_2 NTs were carried out at 50°C using a potentiostat/galvanostat (Autolab PGSTAT 30, Eco Chemie BV) connected to a three-electrode cell (K0269A Faraday Cage, PAR) where TiO_2-NTs, platinum and Ag/AgCl were used as the working, the counter and reference electrodes, respectively. The electrolyte bath was composed of 0.1 M $CuSO_4$ and 0.75 M lactic acid and then adjusted to pH = 9 using 5 M NaOH solution. The deposition process was performed at a cathodic potential of -0.6 V (vs Ag/AgCl) for different durations with magnetically stirring the solution at 50°C [37]. After every electrodeposition, the obtained Cu_2O/TiO_2-NTs samples were rinsed with deionized water and then dried in air at room temperature. We achieved 8 samples by varying the electrodeposition time starting from 50s until 300s considering the pure TiO_2 sample and referenced as Cu_2O/TiO_2-NTs-50s, Cu_2O/TiO_2-NTs-75s, Cu_2O/TiO_2-NTs-100s, Cu_2O/TiO_2-NTs-150s, Cu_2O/TiO_2-NTs-200s, Cu_2O/TiO_2-NTs-250s and Cu_2O/TiO_2-NTs-300s.

2.2. Evaluation of the photocatalytic activity of Cu_2O/TiO_2-NTs during adsorption and decomposition of butane-2, 3-Dione

The Cu_2O-NPs/TiO_2-NTs catalyst – based degradation of Butane-2, 3-dione (BUT: $C_4H_6O_2$), 99% purity (Janssen chimica) was achieved in a specific reactor. The photocatalytic experiments were carried out using a 250 mL spherical batch reactor. A Sylvania CF-L 24W/840 source with a spectral emission in visible range (380 - 720) nm, which are used in

our previous work [7], could be inserted outside the reactor from above. The variation of the BUT concentration and its oxidation by-products were measured using a gas chromatograph (Clarus GC-500) equipped with a flame ionization detector (FID). The chromatograph is also equipped with an apolar capillary DB-MS column having a length of 60 m and a diameter of 0.25 mm (the film thickness is 0.25 µm). The detector (FID) operates with a mixture of air and hydrogen (H_2), Helium (He) was used as a carrier gas with a flow rate of 1mL/min. The analysis conditions, like oven temperature was initially kept at 50°C for 3 min and was programmed to rise 100°C at 2°C/min, outstanding at the maximum temperature for 10 min subsequently. Injection and detection temperatures, were kept at 250°C for both, and were used to quantify the Inlet and Outlet BUT concentrations. A volume of 500 µL of the catalyzed samples (BUT) is injected manually with a gas-tight syringe and this procedure is repeated at least three times.

2.3. Antibacterial test

To investigate the antibacterial activity of Cu_2O-NPs/TiO_2-NTs, *Escherichia coli* (*E. coli*) was selected as probe. An initial concentration of 100 µL culture aliquots with ~ 1.85 10^8 colony-forming unit per milliliter (CFU/mL) was placed on the catalyst surface. The bacteria sample was spread on the catalyst surface and illuminated by the same radiation source. After preselecting the photocatalysis times (1h, 2h, 3h, 5h, 7h), the bacterial suspensions (inoculum) were recovered from the catalyst surface using tween solution. Serial dilutions were performed with tryptone salt broth to facilitate the bacterial counting. Subsequently, 100 µL of dilute solution was placed on petri dishes containing a nutrient solution (tests were twice for each dilution) and placed in an incubator for 24 hours at 37 °C to determine the number of bacterial colonies. After incubation, the colonies or CFU (Colonies Forming Units) formed on the surface of the culture medium were counted visually for dishes containing between 0 and 300 colonies. These dishes correspond to those obtained from two successive dilutions and at least one dish has at least 15 colonies visible on the surface of the culture medium after incubation (at the maximum 4 dishes). Dishes with more than 300 colonies visible on the surface of the culture medium after incubation are not exploitable. The number of CFU “C” on the used dishes was calculated using the following formula:

$$C = \sum_{i=1}^{i=4} C\mathrm{i};$$

With $\sum_{i=1}^{i=4} C\mathrm{i}$ is the sum of the counted colonies on selected dishes.

The concentration “N” (CFU/mL) of cultivable bacteria in the test samples was calculated using the following formula:

$$N = \frac{\sum C}{\mathrm{V}(n_1 + 0.1n_2)\mathrm{d}}$$

With C is the UFC number on the used dishes, V is the volume of the suspension spread on the surface of the Petri dishes (in ml), n_1, n_2 are the number of retained dishes at first and second dilution respectively, and d is the dilution ratio corresponding to the lowest retained dilution.

2.4. Characterizations of Cu_2O-NPs/TiO_2NTs

X-ray diffraction (XRD) analyses were performed with an X-ray diffractometer (Philips X'PERTMPD) using the Cu Kα irradiation, λ = 1.5406 Å. The diffraction data was gathered over the diffraction angle range of 20° - 80° with a scanning step of 0.016°. The surface morphology of the Cu_2O-NPs/TiO_2-NTs samples was examined by scanning electron microscope (SEM, Jeol JSM-6300) and FEI Tecnai G2 transmission electron microscopy (TEM) operating at 200 kV with a LaB6 filament. The chemical composition analysis was performed using the energy dispersive X-ray spectroscopy (EDXS) system attached to the TEM. The photoluminescence (PL) spectra were measured on the Cu_2O-NPs/TiO_2-NTs samples using a fluorescence spectrophotometer (Perkin Elmer LS55) equipped with a xenon lamp at an excitation wavelength of λ = 340 nm. The total reflectivity spectra of the Cu_2O/TiO_2-NTs Nano-hybrids were recorded using a UV-Vis-IR spectrometer.

3- Results and discussion

3.1. Results of characterizations of Cu_2O-NPs/TiO_2NTs

Figure 2 shows SEM top view of the TiO_2-NTs catalyst before (Fig. 2a) and after electrodeposition of Cu_2O-NPs at 250s and 300s (Figs 2b and 2c).

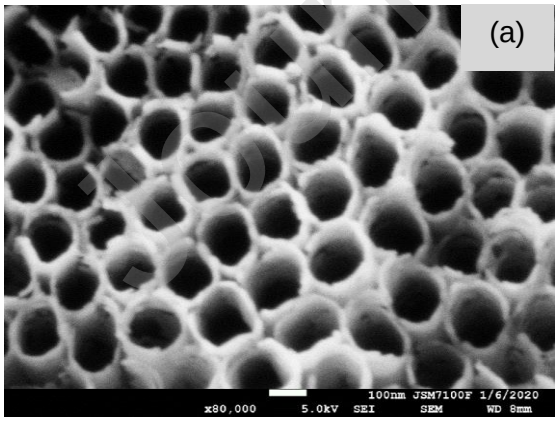

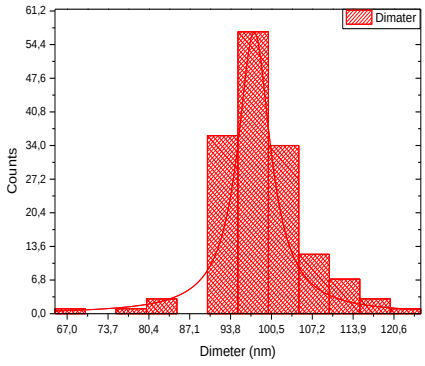

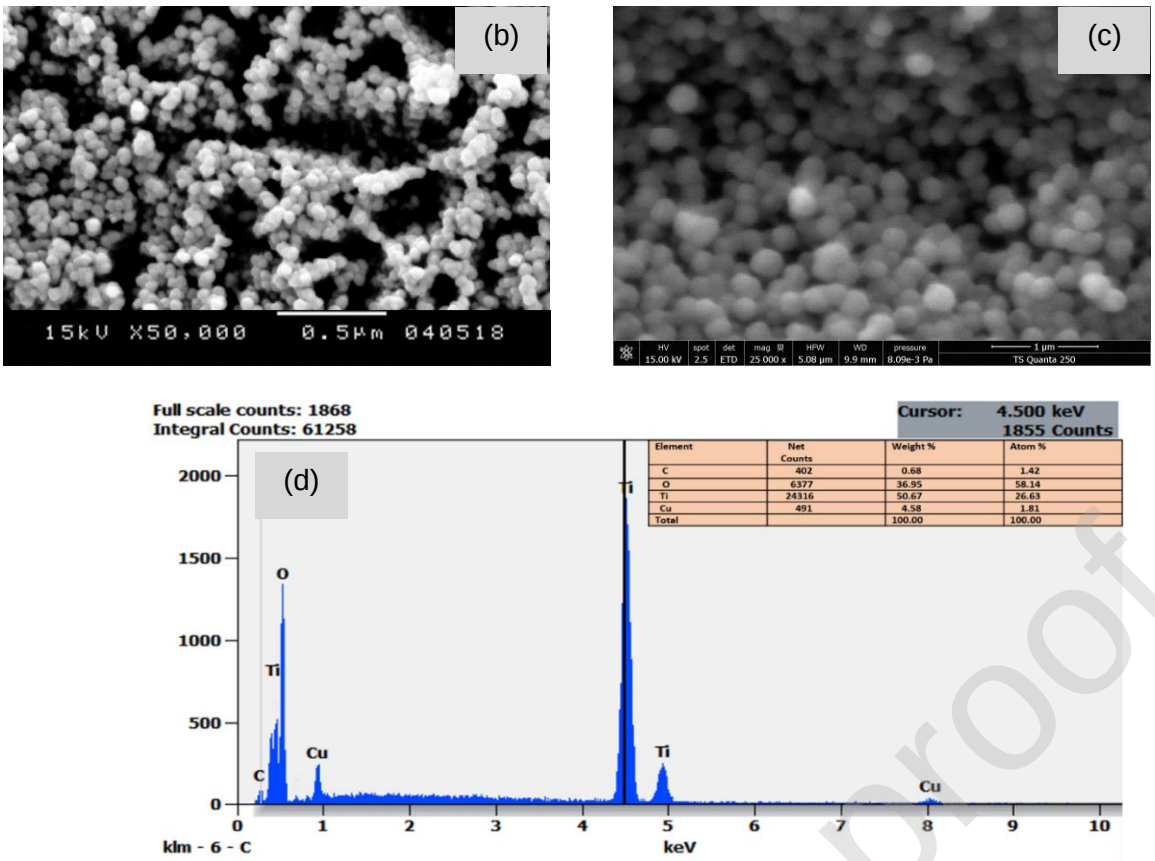

Figure 2: Typical SEM top-view images of TiO_2-NTAs (a) before and (b) after their decoration by Cu_2O-NPs at 100s and (c) at 300s, (d) EDS Spectra of Cu_2O-NPs/TiO_2-NTs-250s. The histogram shows the diameter distribution of the TiO_2-NTs electrodeposited at 100s.

Untreated TiO_2-NTs are composed of highly ordered and aligned NTs perpendicular to the Ti substrate; the average diameter of the NTs at 100s electrodeposition time is about 100 nm (histogram in Fig. 2b). Almost uniformly dispersed Cu_2O-NPs (Figs. 2b and 2c) are formed at 100s and 300s electrodeposition times. The increase of the electrodeposition time from 100s to 300s leads to the aggregation of the Cu_2O-NPs together with an increase of their average diameter size (Fig. 2b & 2c). Figure 2d depicts the EDS analyses of Cu_2O-NPs/TiO_2-NTs electrodeposited at 250s. We may notice the presence of Cu, O and Ti elements (Fig. 2d), however at this stage we cannot conclude to the formation of crystallized stoichiometric Cu_2O NPS since oxygen exists in both TIO_2 and Cu_2O. In order to confirm the existence of crystalline Cu_2O NPs, we performed TEM and HRTEM analyses. Figure 3a and its inset show TEM mages of TiO_2-NTs decorated by Cu_2O-NPs at 100s electrodeposition time. One may notice the presence of Cu_2O-NPs with arbitrary forms on the walls of the TiO_2-NTs. The smaller sized Cu_2O-NPs (Cu_2O-NPs size smaller than the TiO_2-NTs opening diameter) are inside the nanotubes, while larger Cu_2O-NPs (size larger than the TiO_2-NTs opening diameter (size of Cu_2O-NPs > 100 nm)) are on the edge of the NTS walls (Fig 3.a).

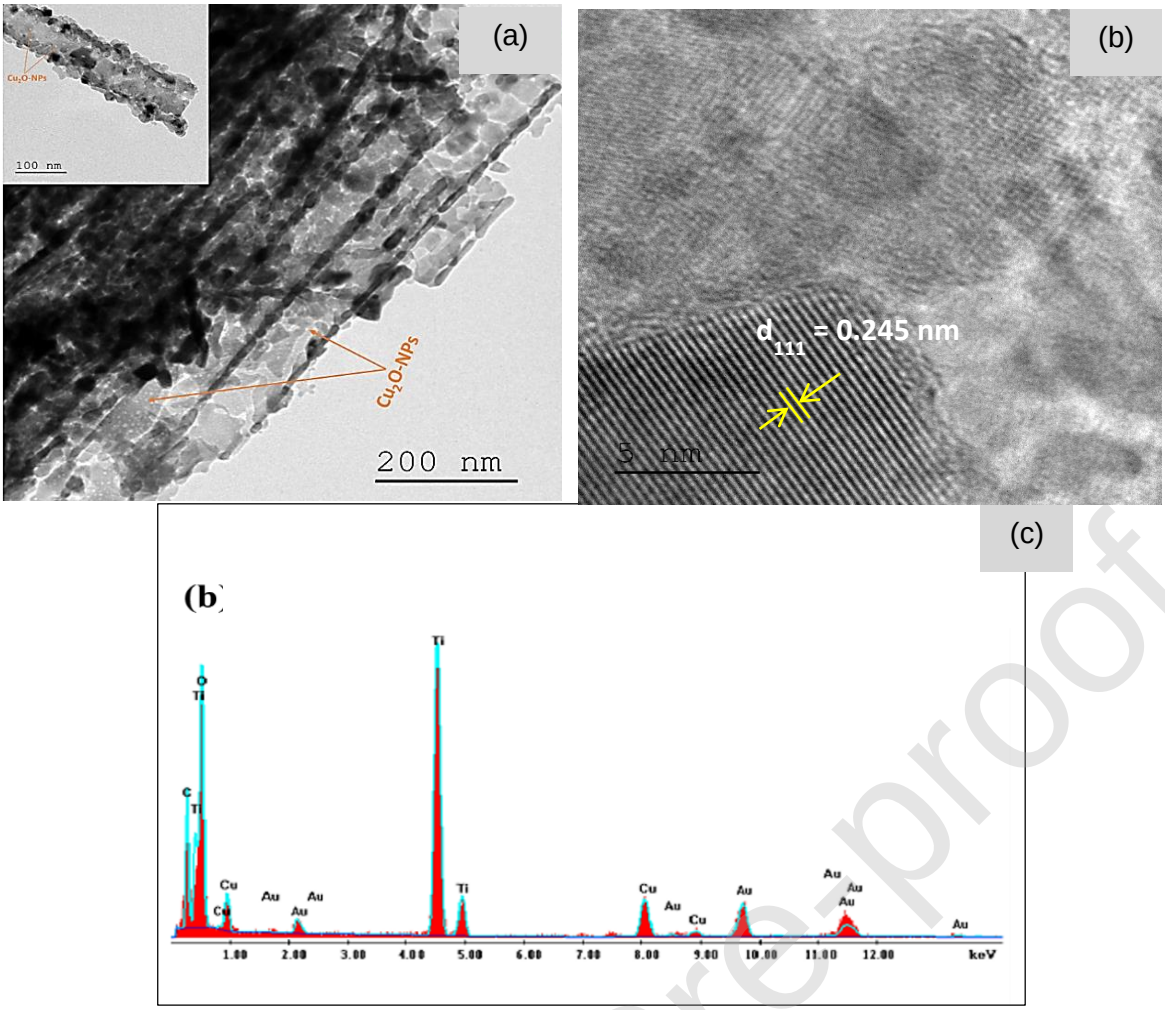

Figure 3: Typical TEM micrograph of TiO_2-NTs decorated with Cu_2O-NPs at (a) 100s electrodeposition time, (b) corresponding HRTEM and (c) the corresponding EDX Spectrum.

In fact, the external Cu_2O NPs growing on the edge of the TiO_2 NTS tend (over time) to block the entry of the NTS blocking further nucleation and growth of the internal Cu_2O NPs (there is an insignificant supply of matter), while the external NPS continue to grow; this could explain the size difference between external and internal Cu_2O NPS.

Figure 3b shows HRTEM image of the Cu_2O-NPs. It is worth noting the existence of well-crystallized Cu_2O NPs having a (111) oriented crystallographic planes. The EDX analysis (Fig. 3c) shows the presence of Au, O, Ti and Cu elements in the Cu_2O-NPs/TiO_2-NTs. The presence of Au is due to the use of a gold grid.

Figure 4 shows X-ray diffraction (XRD) patterns of pure TiO_2-NTs and Cu_2O-NPs/TiO_2-NTs. XRD patterns (Fig. 4a) confirm that all TiO_2-NTs are crystallized in the anatase phase. All diffraction peaks related to Cu_2O are indexed according to the JCPDS card (No. 78-2076).

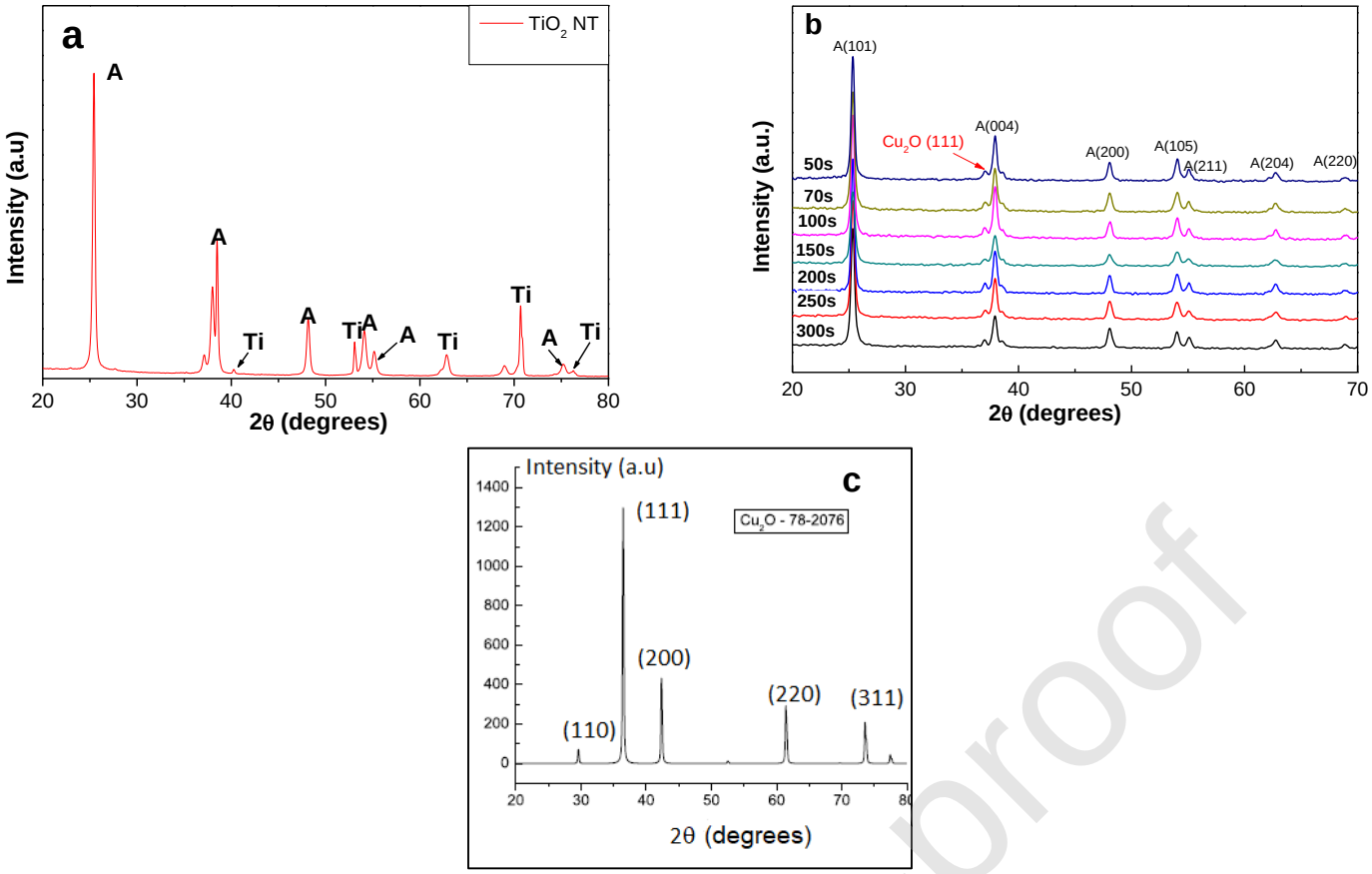

Figure 4: XRD patterns of TiO_2-NTs (a) before and (b) after decoration with Cu_2O-NPs as a function of deposition, (c) XRD of Cu_2O (JCPDS card No. 78-2076).

One may notice that only XRD peak related to the (111) crystallographic orientation of Cu_2O (appearing at $2\theta = 37°$) is detectable; in good agreement with HRTEM (Fig. 3b). The (111) XRD peak is the most intense one whatever the electrodeposition time may be. The (111) XRD peak is also the highest one in the corresponding Cu_2O XRD powder (Fig. 3c, JCPDS card No. 78-2076), indicating that the electrodeposition process does not favor any crystallographic orientation. The disappearance of the other Cu_2O NPs XRD peaks is mainly due to the strong predominance of TiO_2 as compared to the insignificant quantity of the dispersed Cu_2O NPs.

The optical properties of Cu_2O-NPs/TiO_2-NTs prepared at different electrodeposition time were studied by measuring their reflectance diffuse spectra (DRS). From the DRS, the absorption spectra were calculated approximately by the Kubelka-Munk function [49]:

$\boldsymbol{F(R)} = \frac{(1-R)^2}{2R}$ = α; where R is the diffuse reflectance,

Figure 5a shows the UV-VIS absorption spectra of the Cu_2O/TiO_2-NTs nanocomposites for different deposition times (200s, 250s and 300s). The energy band structure of the pure TiO_2-NTs offers a strong optical absorption in the ultraviolet range ($\lambda < 400$ nm) (Fig. 5a). The increase of the optical absorption of the Cu_2O/TiO_2-NTs nanocomposites in the 400 -

450 nm optical range (energy > 2.75 eV) is mainly due to interfacial charge transfer from the TiO_2-NTs to the Cu_2O-NPs, as Cu_2O absorbs below 2.3 eV [43 – 46]. However, the weak absorption near 500 nm (~ 2.5 eV) is due inter-band-based absorption in Cu_2O. The increase of the absorbance beyond a deposition time of 200s is due to further aggregation of the Cu_2O-NPs, which become larger and larger as the deposition time increases (Figs 2b & 2c).

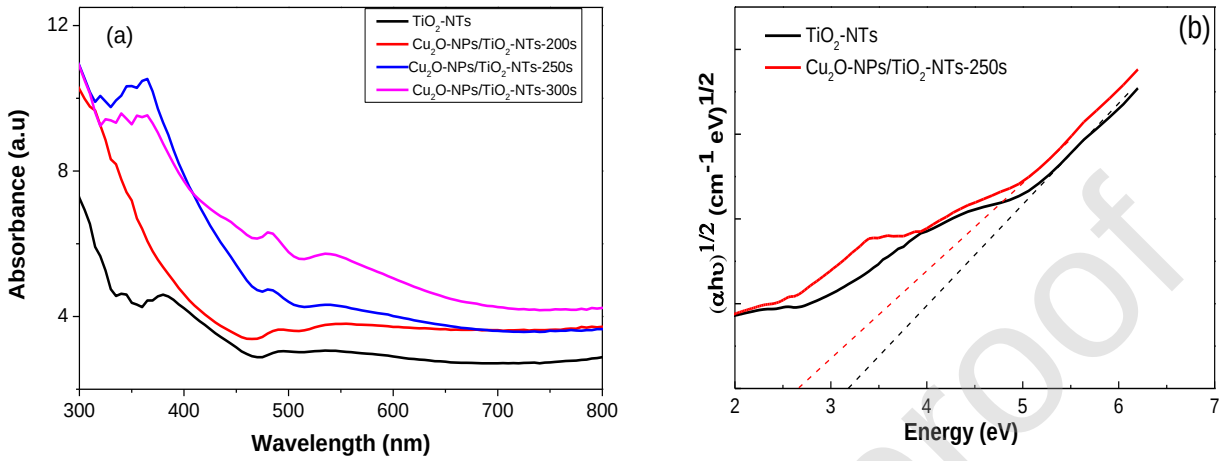

Figure 5: (a) UV-VIS diffuse reflectance spectra of Cu_2O-NPs/TiO_2-NTs at different deposition times, (b) the plots of $(\alpha h\nu)^{1/2}$ versus $(h\nu)$ for pure TiO_2-NTs and Cu_2O-NPs/TiO_2-NTs-250s

The band gap of pure TiO_2-NTs and Cu_2O-sensitized TiO_2-NTs (Cu_2O-NPs/TiO_2-NTs) were deduced from figure 5a by considering the Tauc plots $((\alpha^*h\upsilon)^n$ vs $h\upsilon)$, where α is the absorption coefficient. The optical band gap of the Cu_2O sensitized TiO_2-NTs was found to be indirect and has a value (2.68 eV) slightly shifted from that of pure TiO_2-NTs (3.2 eV). This band gap is larger than that of pure Cu_2O and smaller than that of pure TiO_2-NTs, indicating that Cu_2O-NPs loading may reduce the optical band gap of TiO_2 NTs (Fig. 5-b). Table 1 shows the energy gaps and the corresponding wavelength of pure TiO_2-NTs and Cu_2O-NPs sensitized TiO_2-NTs-250s.

Figure 6 shows the photoluminescence (PL) spectra of TiO_2-NTs and Cu_2O-decorated TiO_2-NTs at different electrodeposition times in the 380 nm - 650 nm wavelength range. The PL spectrum gives further information on recombination and migration of photogenerated electron-hole pairs. To investigate the luminescent defect states of the prepared samples, we used a 340 nm wavelength radiation as excitation. The PL of Cu_2O-sensitized TiO_2-NTs (200s and 250s) has lower PL intensities than pure TiO_2-NTs. In fact, the recombination rate of photogenerated electrons-holes pairs in TiO_2 NTs decreases until Cu_2O-NPs deposition time of 250s. For 300s deposition time the PL intensity increases, probably due to higher Cu_2O NPs concentration, this variation may also be related to the variation of the energy

gap of Cu_2O-NPs, which influences the electrons-holes pairs separation, therefore the recombination rate and consequently the PL intensity of the TiO_2-NTs.

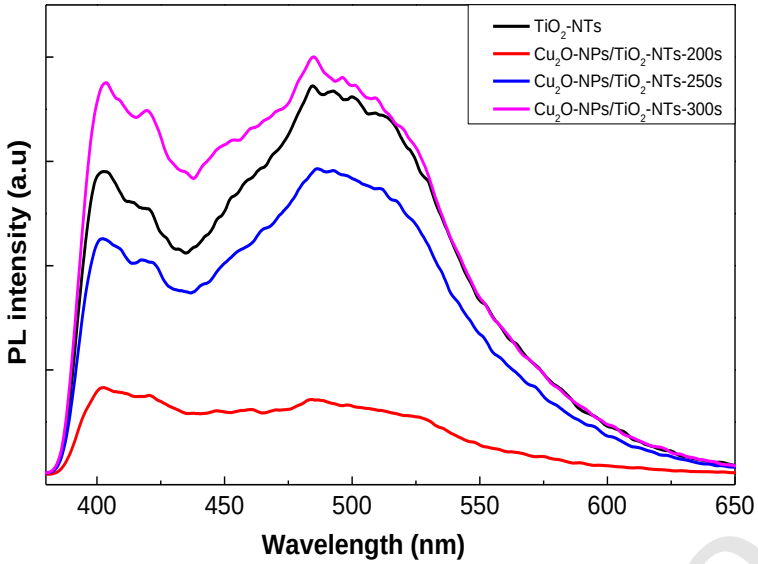

Figure 6: Photoluminescence spectra of TiO_2-NTs and Cu_2O-NPs/TiO_2-NTs at different deposition times.

3.2. UV-Visible-assisted oxidation tests

3.2.1. Oxidation of butane-2, 3-Dione

The photocatalytic performances of TiO_2-NTs and Cu_2O-NPs/TiO_2-NTs at different deposition times (200s, 250s, 300s) were evaluated throughout BUT degradation under visible light irradiation. The catalysts (dimensions: 1.2 cm x 2.5 cm) are placed at the bottom of the photocatalytic reactor. The initial BUT concentration was set at 4.4 g / m^3. Before lighting the lamp, the assembly is kept in the dark for one hour in order to reach the adsorption-desorption balance between the pollutant butane-2, 3-dione (BUT) and the catalyst.

Figure 7 shows that Cu_2O-sensitized TiO_2-NTs has higher photocatalytic activity on BUT than pure TiO_2-NTS, whatever at the electrodeposition time may be. It is clearly seen (Fig. 7) that BUT degradation increases with increasing Cu_2O-NPs deposition time, it reaches 99.1% within 7 hours at 250s electrodeposition time. However, only ~ 71.9% of BUT degrades at 300s electrodeposition time. The relatively low BUT degradation at 300s (compared to 200s) could be due to Cu_2O NPs aggregation, which in turn decreases the active sites on the catalyst surface close to the TiO_2 NTs openings, preventing the transfer and separation of the charge carriers and then decreases the photocatalytic activity [52]. It has been shown elsewhere that smaller nanoparticle sizes lead to an excellent charge transfer and the to an enhanced photocatalytic activity [52,53].

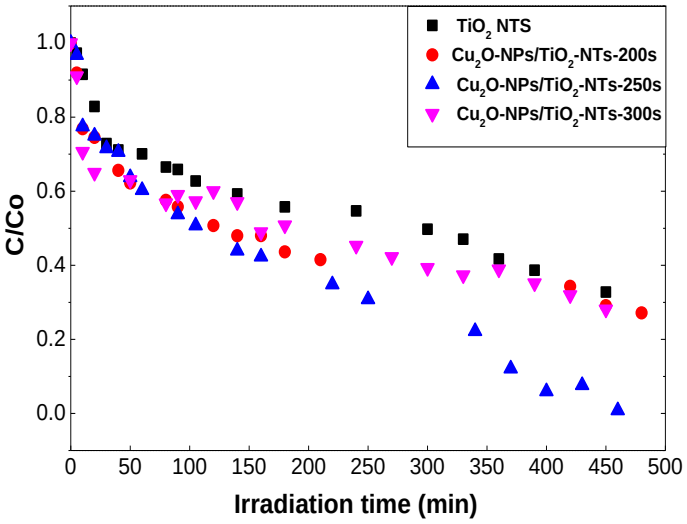

Figure 7: Variation of the concentration of BUT using TiO_2-NTs and Cu_2O-NPs/TiO_2-NTs at different deposition time.

The efficient photocatalytic performance of Cu_2O-NPs/TiO_2-NTs as regard to TiO_2-NTs can mainly be explained by the energy levels of both semiconductors (Fig. 1), which leads to better photoresponse in the visible light range, thus reducing the recombination of electron-hole pairs. The band gap energy of Cu_2O-NPs is around 2.1 eV and its conduction band has a potential, which is worth - 1.4 eV [54] and higher than that of TiO_2 (potential of CB - 0.2 eV) [55]; in these conditions electrons excited in the Cu_2O-NPs conduction band can be transferred to the conduction band of TiO_2 after excitation by UV-Visible light. On the contrary, holes formed in the valence band of TiO_2-NTs migrate towards the valence band of the Cu_2O-NPs, thus accelerating the separation of the photogenerated electron-hole pairs in the semiconductors (Cu_2O and TiO_2). On the other hand, the photogenerated electrons effectively reduce the atmospheric oxygen species through a multi-electron reduction process, while holes in the valence band decompose the COV pollutant (BUT) due to their strong oxidation power [56]. This result is in agreement with previous results [44, 57].

Figure 8 shows the variation of BUT concentration versus irradiation time at different inlet concentration using the Cu_2O-NPs/TiO_2-NTs-250s catalyst. The initial degradation rate (t = 0) decreases as the inlet BUT concentration increases (Fig. 8); this behavior is due to higher availability of photocatalytic sites at a low initial concentration [58, 59]. In fact, the number of molecules effectively participating in the reaction do not increase proportionally with the inlet concentration, thus resulting in a decrease of the degradation efficiency, which would be due to the limited adsorption capacity of the active sites at the catalyst surface.

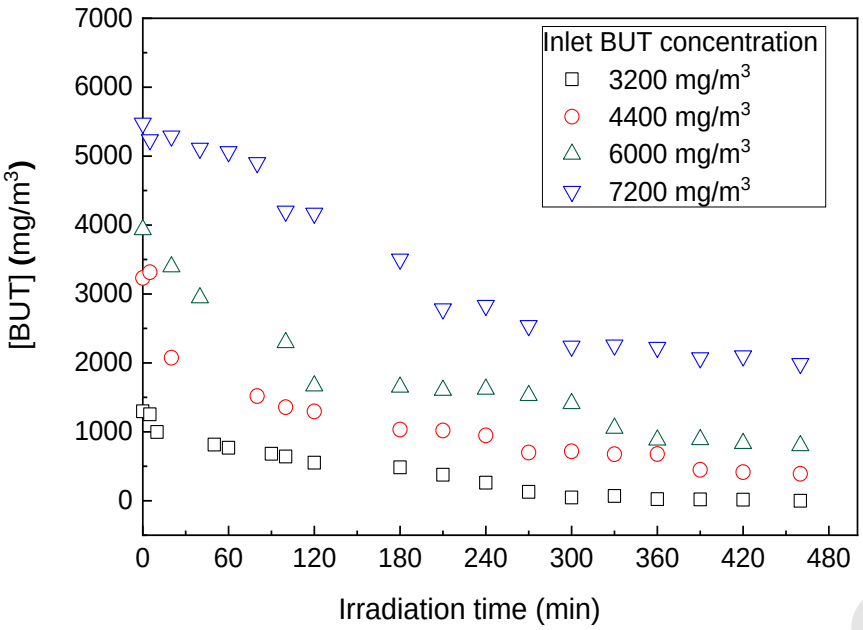

Figure 8: BUT degradation versus inlet BUT concentration using Cu_2O-NPs/TiO_2-NTs-250s

In order to describe the photocatalytic performance of Cu_2O-NPs/TiO_2-NTs-250s, we used the Langmuir-Hinshelwood model (L-H) equation [59]:

$$r_0 = -\frac{d[VOC]}{dt} = k_c \frac{K[VOC]_0}{1 + K[VOC]_0}$$

Where r_0 (mmol/g_{cat} m^3 s) is the initial photocatalytic degradation rate, [**VOC**] is the initial BUT concentration (mmol/m^3), ***K*** is the adsorption constant (m^3/mmol) and $\boldsymbol{k_c}$ is the kinetic constant (mmol.m^{-3} s g_{TiO2}) at maximum coverage of the experimental conditions.

The plot of $1/r_0$ versus $1/[COV]_0$ (Fig. 9) allows to determine $\boldsymbol{k_c}$ and ***K*** values. The linearized (L-H) equation is:

$$\frac{1}{r_0} = \frac{1}{k_c K} \times \frac{1}{[VOC]_0} + \frac{1}{k_C}$$

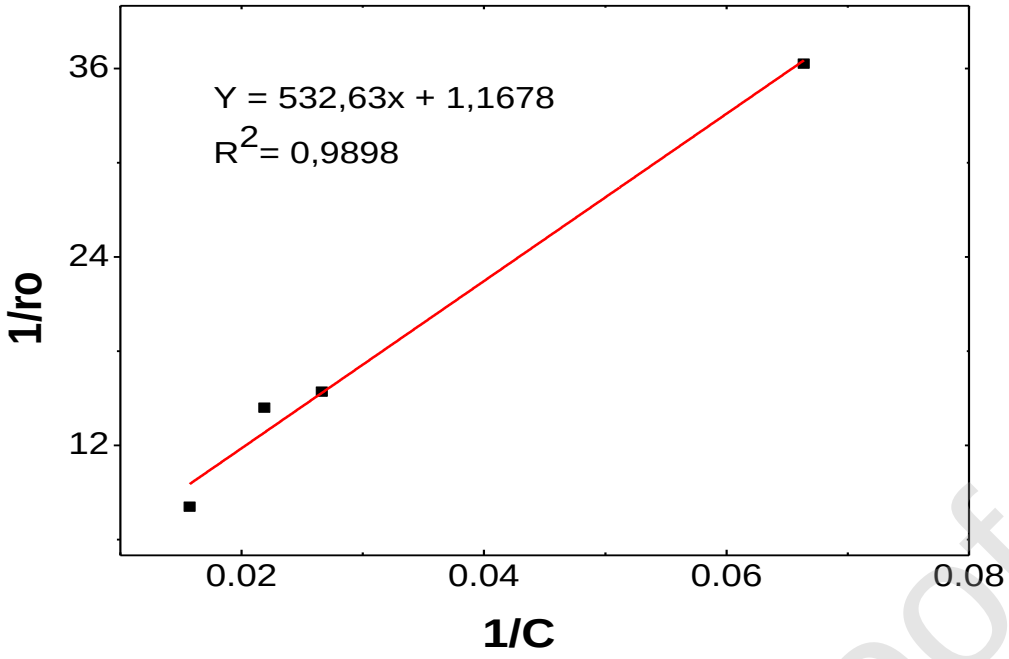

Figure 9: Linear regression using L-H model for BUT degradation on Cu_2O-NPs/TiO_2-NTs-250s catalyst

The kinetic and the adsorption constant of L-H values are summarized in the table 2. The results showed that the Cu_2O-modified TiO_2 NTs leads to a faster COV removal compared to other types of catalysts such as TiO_2 impregnated polyester (PES) and glass fiber (GFT)-TiO_2 (GFT-TiO_2, PES-TiO_2) [59], and has a kinetic constant of 0.85 $mmol.m^{-3}$ $s.g_{TiO2}$. Table 2 gives the kinetic and the adsorption constants referring to the (L-H) model.

3.2.2 Simultaneous oxidation of butane-2, 3-dione and bacteria

In order to investigate the antibacterial aspect of Cu_2O-sensitized TiO_2-NTs in terms of E. coli inactivation and in term of simultaneous removal of E. coli and BUT, several experiments were done with Cu_2O-NPs/TiO_2-NTs-250s catalyst with an initial bacterial concentration of ~1.86 10^8 (CFU/mL). Figure 10 shows the antibacterial activity of Cu_2O-NPs/TiO_2-NTs-250s with and without BUT under visible light. We found that there is almost no effect of photolysis and VOC on bacteria cells inactivation (Fig. 10). The use of Cu_2O-NPs/TiO_2-NTs-250s catalyst has an *E. coli* inactivation rate of about ~ 99.8% with COV and 99.59% without COV within 60 min of light irradiation. This inactivation rate is about twice fast than TiO_2-NTs catalyst (46.44%).

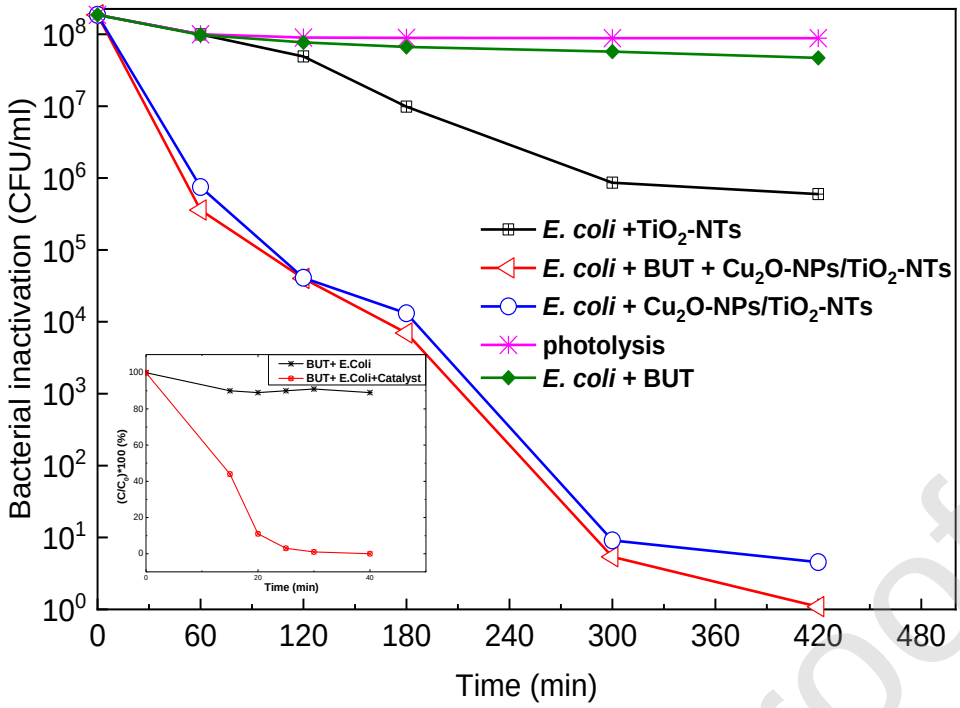

Figure 10: E. coli inactivation rate with and without BUT using the Cu_2O-NPs/TiO_2-NTs-250s catalyst. The initial concentration of E. coli is ~1.86 10^8 CFU/mL). The inset in Fig. 10 shows BUT amount present in the reactor in the presence and absence of Cu_2O-NPs/TiO_2-NTs-250s catalyst.

BUT respiration by the bacterial cells during the photocatalytic process (inset in Fig. 10) and by-products resulting from the VOC degradation can affect the bacterial cells but not in a remarkable way. The high antibacterial activity of Cu_2O-modified TiO_2 NTs is due to the antibacterial properties for each semiconductor alone [60, 61], and to the combination of the TiO_2 NTs and Cu_2O effects. These results are almost similar to those of our previous work, where we studied the effect of Ag-NPs on the antibacterial activity of TiO_2-NTs [62]. In fact, Ag-decorated TiO_2-NTs enhanced E. coli inactivation via localized plasmon resonance (LSPR) and oxidation of the Ag-NPs in AgO and Ag_2O, hence improving the transfer and separation of the charge carriers; we obtained a bacterial inactivation of 99.99 % within 90 min. After irradiation with visible light, the intrinsic activity of Cu(I) is enhanced in accordance with the literature [61], where it has been shown that Cu_2O presents a high bacterial inactivation capability. In other words, light irradiation could stimulate electron transfer between Cu and bacterial cells and products a reactive oxygen species (ROS) resulting in the bacterial cells inactivation [61]. Sunada et al. [63] reported that the contact between Cu species and bacterial cells can extract electrons from cells, which leads to proteins denaturation. In addition, TiO_2-NTs present a good antibacterial activity under UV irradiation [60], due to the photogeneration of electron/hole pairs resulting in ROS generation ($OH^{\bullet}$, $O_2^{-\bullet}$…) [53]. Min Cho et al. reported that free and surface bound hydroxyl radicals present

a main pathway in *E. coli* inactivation [64, 65]. On the other hand, any damage to the surface of the bacterial cells, such as respiration or other active systems, can destroy the metabolic systems of the bacteria, leading to less active oxygen species ($O_2^{-\bullet}$ and $^{\bullet}OH$) to play a role in the bacterial inactivation [64]. Thus, the of Cu_2O-NPs /TiO_2-NTs photocatalyst has higher photocatalytic activity as compared to pure TiO_2-NTs. This improvement is due to the adequate difference in the energy levels of their conduction and valence bands. Indeed, the energy position of the Cu_2O conduction band is higher than that of the TiO_2-NTs conduction band [66], so that the photoexcited electron (e^-) in the Cu_2O-NPs conduction band (CB) can swiftly transferred to the TiO_2-NTs under UV-Visible illumination (Eq. (2)), thus accelerating separation of the photogenerated electrons and holes and hence inhibiting their recombination. The photoexcited electrons can migrate from the CB of the Cu_2O-NPs to the TiO_2-NTs CB where it would react with absorbed O_2 (Eq (3)), thus contributing to the formation of $^{\bullet}O^-_2$ radicals. Many oxidizing radicals, such $^{\bullet}OH$, can be generated following the reaction of superoxide radicals and H^+ ions. The photocatalytic reaction has been described in a previous work [7] and can be summarized below according to the main equations:

$$Cu_2O + h\nu\ (< 3.1\ eV) \rightarrow Cu_2O\ (e^-_{CB}) + Cu_2O\ (h^+_{VB}) \quad (1)$$

$$e^-_{cb} + TiO_2 \text{ or } (Ti^{4+}) \rightarrow TiO_2^- \text{ or } (Ti^{3+}) \quad (2)$$

$$Ti^{3+} + O_2 \rightarrow Ti^{4+} + {}^{\bullet}O_2^- \quad (3)$$

$$TiO_2 + h\nu\ (> 3.1\ eV) \rightarrow TiO_2\ (h^+_{VB}) + TiO_2\ (e^-_{CB}) \quad (4)$$

$$^{\bullet}O_2^- + H^+ \rightarrow HO_2^{\bullet} \quad (5)$$

$$HO_2^{\cdot} + H^+ + e^-_{CB} \rightarrow H_2O_2 \quad (6)$$

$$H_2O_2 + e^-_{cb} \rightarrow OH + OH^- \quad (7)$$

$$h^+_{VB}\ (Cu_2O \text{ or } TiO_2) + \text{bacteria/COV} \rightarrow CO_2, H_2O, N, S \quad (8)$$

Finally, COV molecules and bacterial cells are oxidized and decomposed by these powerful active ROS. Figure 11 summarizes the mechanism of the photocatalytic activity:

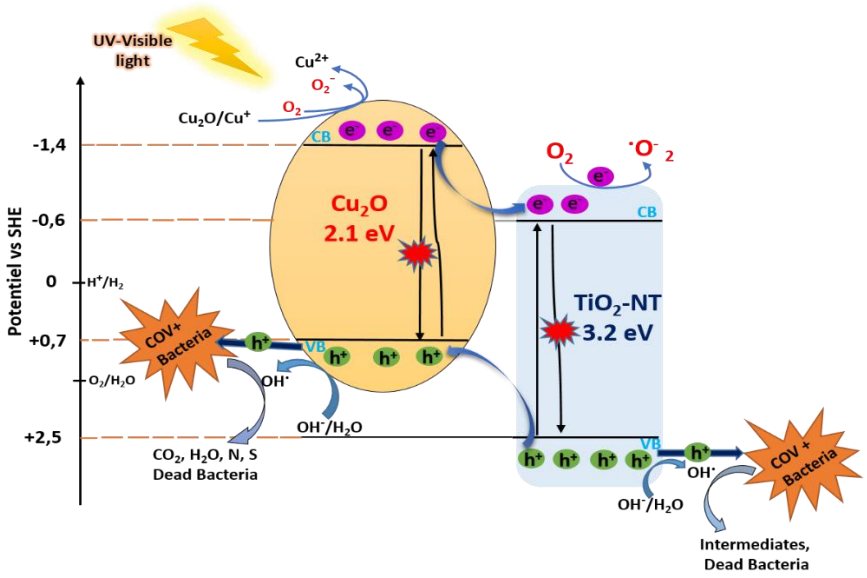

Figure11: Suggested mechanism for Butane-2,3-dione and E. coli removal and charge transfer in Cu_2O-NPs/TiO_2-NTs heterojunction under UV-Visible light irradiation.

4- Conclusion

Cu_2O-NPs/TiO_2-NTs nanocomposites were successfully achieved using electrochemical anodization of titanium and electrochemical deposition of Cu_2O-NPs on TiO_2-NTs at different deposition times. The TiO_2-NTs are composed of homogenous nanotubes having a diameter of 100 nm and crystallized in anatase phase. The deposition of the Cu_2O NPs was made by varying the electrodeposition time from 50s to 300s. The adjunction of Cu_2O-NPs to the TiO_2-NTs leads to an increase of the visible light absorption up to around 500 nm. TiO_2-NTs, and Cu_2O-NPs/TiO_2-NTs (with different electrodeposition times) were tested for the removal of a Volatile Organic Compound (VOC - BUT) under exposition to visible light (380 - 720nm). Other tests were carried out for both degradation of Volatile Organic Compounds and bacteria (E. Coli) inactivation. At an optimized Cu_2O-NPs electrodeposition time (Cu_2O-NPs/TiO_2-NTs-250s) the catalyst exhibits a high photocatalytic efficiency for both BUT removal and bacteria inactivation. Nearly total inactivation of bacteria was achieved using the same photocatalyst (Cu_2O-NPs/TiO_2-NTs-250s) for one hour of light irradiation. Also, we note that simultaneous treatment of VOC and bacteria leads to a 99.7% bacterial inactivation and a complete removal of VOC within 60 min and 25min of light irradiation, respectively. This high photocatalytic efficiency is attributed to a combination of high visible light absorption of Cu_2O nanoparticles and to the positions of the energy band levels of both semiconductors. This photocatalyst system shows great enhancement of VOC degradation, bacteria cells killing as regard to the sole TiO_2-NTs together with simultaneous treatment of VOC and bacteria due to the efficient transfer of the photogenerated electrons-holes pairs

and to the extended photoresponse in the UV-Visible range. The Cu_2O-NPs/TiO_2NTs nanocomposites are very stable under light irradiation.

Interest Statement

This manuscript treats a serious environmental problem (contamination of the indoor environment. This problem touches modern society spending more than 70% of their time indoor. The main objective of our manuscript is to investigate the photocatalytic removal of VOCs and bacteria inactivation under semi-real conditions.

Many innovative/unreported findings are presented in this paper.

Here, indoor air from food industries butadiene and Escherichia coli (E. coli) were treated using a recently patented reactor. Moreover, a new specific Cu_2O-NPs decorated TiO_2 nanotubes, suitable for chemical/microbiological applications were tested.

These new findings will promote the development of novel compactness and economical technologies for the multi-contaminated air treatment.

References

[1] B. F. Yu, Z. B. Hu, M. Liu, H. L. Yang, Q. X. Kong, Y. H. Liu, Review of research on air-conditioning systems and indoor air quality control for human health. International journal of refrigeration, 32 (2009) 3-20.

[2] P. K. Nag, Characteristics of Indoor Environmental Quality. Office Buildings 2019: pp. 279-310. Springer, Singapore.

[3] A. A. Assadi, A. Bouzaza, D. Wolbert, Photocatalytic oxidation of trimethylamine and isovaleraldehyde in an annular reactor: Influence of the mass transfer and the relative humidity. Journal of Photochemistry and Photobiology A: Chemistry, 236 (2012), 61-69.

[4] A. A. Assadi, A Bouzaza, I Soutrel, P Petit, K Medimagh, D Wolbert,A study of pollution removal in exhaust gases from animal quartering centers by combining photocatalysis with surface discharge plasma: from pilot to industrial scale, Chemical Engineering and Processing: Process Intensification 111 (2017) 1-6

[5] A. A. Assadi, A. Bouzaza, D. Wolbert, Study of synergetic effect by surface discharge plasma/TiO_2 combination for indoor air treatment: Sequential and continuous configurations at pilot scale. Journal of Photochemistry and Photobiology A: Chemistry, 310 (2015)148-154.

[6] A. A. Assadi, A. Bouzaza, C. Vallet, D. Wolbert, Use of DBD plasma, photocatalysis, and combined DBD plasma/photocatalysis in a continuous annular reactor for isovaleraldehyde elimination–synergetic effect and byproducts identification. Chemical Engineering Journal, 254 (2014) 124-132.

[7] M. Abidi, A. A. Assadi, A. Bouzaza, A. Hajjaji, B. Bessais, S. Rtimi, Photocatalytic indoor/outdoor air treatment and bacterial inactivation on Cu_xO/TiO_2 prepared by HiPIMS on polyester cloth under low intensity visible light. Applied Catalysis B: Environmental, 259 (2019) 118074.

[8] A. Rabahi, A. A. Assadi, N. Nasrallah, A. Bouzaza, R. Maachi, D. Wolbert, Photocatalytic treatment of petroleum industry wastewater using recirculating annular reactor: comparison of experimental and modeling. Environmental Science and Pollution Research, 26 (2019) 19035-19046.

[9] W. A. Saoud, A. A. Assadi, M. Guiza, S. Loganathan, A. Bouzaza, W. Aboussaoud, A. Ouederni, S. Rtimi, D. Wolbert, Synergism between non-thermal plasma and photocatalysis: Implicationsin the post discharge of ozone at a pilot scale in a catalytic fixed-bed reactor. Applied Catalysis B: Environmental, 241 (2019) 227-235.

[10] A. Sukmilin, B. Boonchom, C. Jarusutthirak, Catalytic Ozonation using Iron-Doped Water Treatment Sludge as a Catalyst for Treatment of Phenol in Synthetic Wastewater. Environment and Natural Resources Journal, 17 (2019) 87-95.

[11] A. Alinejad, H. Akbari, M. Ghaderpoori, A. K. Jeihooni, A. Adibzadeh, Catalytic ozonation process using a MgO nano-catalyst to degrade methotrexate from aqueous solutions and cytotoxicity studies in human lung epithelial cells (A549) after treatment. RSC advances, 9 (2019) 8204-8214.

[12] T. Kako, F. Ichihara, G. Liu, X. Meng, J. Ye, Study on the enhancement of photocatalytic environment purification through ubiquitous-red-clay loading. SN Applied Sciences, 1 (2019) 138.

[13] K. Sridharan, E. Jang, T. J. Park, Novel visible light active graphitic C_3N_4–TiO_2 composite photocatalyst: Synergistic synthesis, growth and photocatalytic treatment of hazardous pollutants. Applied Catalysis B: Environmental, 142(2013) 718-728.

[14] V. Tamilselvan, K. Sridharan, K. N. Rao, R. Philip, R. Optical nonlinearity in lead sulfide microtowers. Journal of Physics D: Applied Physics, 43 (2010), 385402.

[15] R. Agarwal, C. M. Lieber, C. M, Semiconductor nanowires: optics and optoelectronics. Applied physics A, 85(2006), 209.

[16] A. Vaneski, A. Susha, J. Rodríguez-Fernández, M. Berr, F. Jäckel, J. Feldmann, A. L. Rogach, Hybrid colloidal heterostructures of anisotropic semiconductor nanocrystals decorated with noble metals: synthesis and function. Advanced Functional Materials, 21(2011), 1547-1556.

[17] P. Roy, S. Berger, P. Schmuki, P. TiO_2 nanotubes: synthesis and applications. Angewandte Chemie International Edition, 50 (2011), 2904-2939.

[18] V. Vamathevan, R. Amal, D. Beydoun, G. Low, S. McEvoy, S. Photocatalytic oxidation of organics in water using pure and silver-modified titanium dioxide particles. Journal of Photochemistry and Photobiology A: Chemistry, 148 (2002), 233-245.

[19] Z. Zsilák, E. Szabó-Bárdos, O. Fónagy, O. Horváth, K. Horváth, P. Hajós, P. Degradation of benzenesulfonate by heterogeneous photocatalysis combined with ozonation. Catalysis today, 230 (2014) 55-60.

[20] J. Wang, W. D. Zhang, Modification of TiO_2 nanorod arrays by graphite-like C3N4 with high visible light photoelectrochemical activity. Electrochimica Acta, 71 (2012) 10-16.

[21] J. Hensel, G. Wang, Y. Li, J. Z. Zhang, Synergistic effect of CdSe quantum dot sensitization and nitrogen doping of TiO_2 nanostructures for photoelectrochemical solar hydrogen generation. Nano letters, 10 (2010) 478-483.

[22] M. Motola, M. Baudys, R. Zazpe, M. Krbal, J. Michalička, J. Rodriguez-Pereira, D. Pavliňák, J. Přikryl, L. Hromádko, H. Sopha, J. Krýsa and J. M. Macak. 2D MoS_2 nanosheets on 1D anodic TiO_2 nanotube layers: an efficient co-catalyst for liquid and gas phase photocatalysis. Nanoscale, 11 (2019) 23126.

[23] X. Zhou, N. T. Nguyen, S. Özkan, P. Schmuki, P. Anodic TiO_2 nanotube layers: Why does self-organized growth occur — A mini review. Electrochemistry Communications, 46 (2014) 157-162.

[24] S. W. Shin, J. Y. Lee, K. S. Ahn, S. H. Kang, J. H. Kim, Visible light absorbing TiO_2 nanotube arrays by sulfur treatment for photoelectrochemical water splitting. The Journal of Physical Chemistry C, 119 (2015) 13375-13383.

[25] Jan M. Macak, Martin Zlamal, Josef Krysa, and Patrik Schmuki. Self-Organized TiO_2 Nanotube Layers as Highly Efficient Photocatalysts. Small 3 (2007) 300.

[26] M. Altomare, M. Pozzi, M. AllietaL. G. Bettini, E. Selli, E. H_2 and O_2 photocatalytic production on TiO_2 nanotube arrays: Effect of the anodization time on structural features and photoactivity. Applied Catalysis B: Environmental, 136(2013) 81-88.

[27] G. R. Patzke, F. Krumeich, R. Nesper, Reinhard. Oxidic nanotubes and nanorods—anisotropic modules for a future nanotechnology. Angewandte Chemie International Edition, 41, (2002) 2446-2461.

[28] K. Lee, A. Mazare, P. Schmuki, One-dimensional titanium dioxide nanomaterials: nanotubes. Chemical reviews, 114 (2014) 9385-9454.

[29] Hanna Sopha, Michal Baudys , Milos Krbal, Raul Zazpe, Jan Prikryl, Josef Krysac, Jan M. Macak. Scaling up anodic TiO_2 nanotube layers for gas phase photocatalysis. Electrochemistry Communications 97 (2018) 91–9

[30] M. Radzig, O. Koksharova,I. Khmel,V. Ivanov, K. Yorov, J. Kiwi, S. Rtimi, E. Tastekova, A. Aybush, V. Nadtochenko, Femtosecond spectroscopy of Au hot-electron injection into TiO_2: Evidence for Au/TiO_2 plasmon photocatalysis by bactericidal Au ions and related phenomena. Nanomaterials, 9(2019) 217.

[31] Qingyao Wang, Xiuchun Yang, Dan Liu Lina Chi, Junwei Hou. Ag and CdS nanoparticles co-sensitized TiO_2 nanotubes for enhancing visible photoelectrochemical performance. Electrochimica Acta, 83 (2012) 140-145.

[32] Qingyao Wang, Xiuchun Yang, Lina Chi, Miaomiao Cui, Photoelectrochemical performance of CdTe sensitized TiO_2 nanotube array photoelectrodes. Electrochimica Acta, 91 (2013) 330-336

[33] H. Zeghioud, A. A. Assadi, N. Khellaf, H. Djelal, A. Amrane, S. Rtimi, S. Photocatalytic Performance of Cu_xO/TiO_2 Deposited by HiPIMS on Polyester under Visible Light LEDs: Oxidants, Ions Effect, and Reactive Oxygen Species Investigation. Materials, 12 (2019) 412.

[34] J. Yu, J. Kiwi, T. Wang, C. Pulgarin, S. Rtimi, S. Evidence for a dual mechanism in the TiO_2/Cu_xO photocatalyst during the degradation of sulfamethazine under solar or visible light: Critical issues. Journal of Photochemistry and Photobiology A: Chemistry, 375 (2019) 270-279.

[35] S. Song, J. Tu, Z. HeF. Hong, W. Liu, J. Chen, Visible light-driven iodine-doped titanium dioxide nanotubes prepared by hydrothermal process and post-calcination. Applied Catalysis A: General, 378 (2010) 169-174.

[36] T. D. Pham, B. K. Lee, Selective removal of polar VOCs by novel photocatalytic activity of metals co-doped TiO_2/PU under visible light. Chemical Engineering Journal, 307 (2017) 63-73.

[37] T. D. Pham, B. K. Lee, Byeong-Kyu. Novel adsorption and photocatalytic oxidation for removal of gaseous toluene by V-doped TiO_2/PU under visible light. Journal of hazardous materials, 300 (2015) 493-503.

[38] S. Sun, J. Ding, J. Bao, C. Gao, Z. Qi, X. Yang, B. He, C. Li, Photocatalytic degradation of gaseous toluene on Fe-TiO_2 under visible light irradiation: A study on the structure, activity and deactivation mechanism. Applied Surface Science, 258 (2012) 5031-5037.

[39] M. Kalbacova, J. M. Macak, F. Schmidt-Stein, C. T. Mierke , and P. Schmuki. TiO_2 nanotubes: photocatalyst for cancer cell killing. Phys. Stat. Sol. (RRL) 2 (2008) 194–196.

[40] T. D. Pham, B. K. Lee, Effects of Ag doping on the photocatalytic disinfection of E. coli in bioaerosol by Ag–TiO_2/GF under visible light. Journal of colloid and interface science, 428 (2014) 24-31.

[41] R. Del Angel, J. C. Durán-Álvarez, R. Zanella, TiO_2 -Low Band Gap Semiconductor Heterostructures for Water Treatment Using Sunlight-Driven Photocatalysis. Titanium Dioxide: Material for a Sustainable Environment. Chapter 16 (2018) p 305.

[42] M. Janczarek, E. Kowalska, On the origin of enhanced photocatalytic activity of copper-modified titania in the oxidative reaction systems. Catalysts, 7 (2017) 317.

[43] C. Wang, J. Wu, P. Wang, Y. Ao, J. Hou, J. Qian, Photoelectrocatalytic determination of chemical oxygen demand under visible light using Cu_2O-loaded TiO_2 nanotube arrays electrode. Sensors and Actuators B: Chemical, 181(2013) 1-8.

[44] L. Liu, W. Yang, Q. Li, S. Gao, J. Shang, J. Synthesis of Cu_2O nanospheres decorated with TiO_2 nanoislands, their enhanced photoactivity and stability under visible light illumination, and their post-illumination catalytic memory. ACS applied materials & interfaces, 6 (2014) 5629-5639.

[45] I. V. Bagal, N. R. Chodankar, M. A. Hassan, A. Waseem, Do-Heyong Kim, Sang-Wan Ryu. Cu_2O as an emerging photocathode for solar water splitting - A status review. International Journal of Hydrogen Energy. 44 (2019) 21351.

[46] H. H. Tran, M. T. Cao, T. K. Nguyen, Y. S. Kim, Photoreduction route for CuO/TiO_2 nanotubes junction for enhanced photocatalytic activity. RSC Advances, 8 (2018) 12420.

[47] L. Wu, K. L. Tsui, N. Swami, G. Zangari, Giovanni. Photoelectrochemical stability of electrodeposited Cu_2O films. The Journal of Physical Chemistry C, 114 (2010) 11551.

[48] A. Hajjaji, S. Jemai, K. Trabelsi, A. Kouki, I. Ben Assaker, I. Ka, M. Gaidi, B. Bessais and M. A. El Khakani. Study of TiO_2 nanotubes decorated with PbS nanoparticles elaborated by pulsed laser deposition: microstructural, optoelectronic and photoelectrochemical properties. J. Mater. Sci: Mater Electron 30 (2019) 20935.

[49] L. Zhao, W. Dong, F. Zheng,L. Fang, M. Shen, Interrupted growth and photoelectrochemistry of Cu_2O and Cu particles on TiO_2. Electrochimica Acta, 80 (2012) 354.

[50] M. Sboui, S. Bouattour, M. Gruttadauria, L.F. Liotta, V. La Parola, S. Boufi, Hybrid paper–TiO_2 coupled with a Cu2O heterojunction: an efficient photocatalyst under sun-light irradiation. RSC Advances, 6 (2016) 86918-86929.

[51] Y. Li, W. Zhang, X. Shen, P. Peng, L. Xiong, Y. Yu, Octahedral Cu_2O-modified TiO_2 nanotube arrays for efficient photocatalytic reduction of CO_2. Chinese Journal of Catalysis, 36 (2015) 2229.

[52] I. Robel, M. Kuno, P. V. Kamat, Size-dependent electron injection from excited CdSe quantum dots into TiO_2 nanoparticles. Journal of the American Chemical Society, 129 (2007) 4136.

[53] L. Xiong, F. Yang, L. Yan, N. Yan, X. Yang, M. Qiu, Y. Yu, Y. Bifunctional photocatalysis of TiO_2/Cu_2O composite under visible light: Ti^{3+} in organic pollutant degradation and water splitting. Journal of Physics and Chemistry of Solids, 72 (2011) 1104.

[54] Y. Wang, J. Tao, X. Wang, Z. Wang, M. Zhang, G. He,Z. Sun, A unique Cu_2O/TiO_2 nanocomposite with enhanced photocatalytic performance under visible light irradiation. Ceramics International, 43 (2017) 4866-4872.

[55] X. Qiu, M. Miyauchi, K. Sunada, M. Minoshima, M. Liu, Y. Lu, D. Li, Y. Shimodaira, Y. Hosogi, Y. Kuroda, K. Hashimoto, Hybrid Cu_xO/TiO_2 nanocomposites as risk-reduction materials in indoor environments. ACS Nano, 6 (2012) 1609-1618.

[56] X. Yang, C. Chen, Cu_2O sensitized flexible 3D-TiO_2 nanotube arrays for enhancing visible photo-electrochemical performance. RSC Advances, 6 (2016) 70978-70983.

[57] L. Zhong, F. Haghighat, C. S. Lee, N. Lakdawala, Performance of ultraviolet photocatalytic oxidation for indoor air applications: systematic experimental evaluation. Journal of hazardous materials, 261 (2013) 130.

[58] W. Elfalleh, A. A. Assadi, A. Bouzaza, D. Wolbert, J. Kiwi, S. Rtimi, Innovative and stable TiO_2 supported catalytic surfaces removing aldehydes under UV-light irradiation. Journal of Photochemistry and Photobiology A: Chemistry, 343 (2017) 96-102.

[59] A. Ahmadi, T. Wu, Inactivation of E. coli using a novel TiO_2 nanotube electrode. Environmental Science: Water Research & Technology, 3 (2017) 534.

[60] M. Janczarek, M. Endo, D. Zhang, K. Wang, E. Kowalska, Enhanced photocatalytic and antimicrobial performance of cuprous oxide/titania: The effect of titania matrix. Materials 11 (2018) 2069.

[61] A. Hajjaji, M. Elabidi, K. Trabelsi, A. A. Assadi, B. Bessais, S. Rtimi. Bacterial adhesion and inactivation on Ag decorated TiO_2-nanotubes under visible light: Effect of the nanotubes geometry on the photocatalytic activity. Colloids and Surfaces B: Biointerfaces, 170 (2018) 92-98.

[62] K. Sunada, M. Minoshima, K. Hashimoto, Highly efficient antiviral and antibacterial activities of solid-state cuprous compounds. Journal of hazardous materials, 235 (2012) 265-270.

[63] M. Cho, H. Chung, W. Choi, J. Yoon, J. Different inactivation behaviors of MS-2 phage and Escherichia coli in TiO_2 photocatalytic disinfection. Appl. Environ. Microbiol. 71 (2005) 270.

[64] M. Cho, H. Chung, W. Choi, Y. Jeyong, Linear correlation between inactivation of E. coli and OH radical concentration in TiO_2 photocatalytic disinfection. Water research, 38 (2004) 1069-1077.

[65] Y. Liu, H. Zhou, H. Chen, J. Li, D. Li, B. Zhou, W. Cai, Enhanced photoelectrochemical properties of Cu_2O-loaded short TiO_2 nanotube array electrode prepared by sonoelectrochemical deposition. Nano-Micro Letters, 2 (2010) 277-284.

Table 1: Energy band gaps and the corresponding absorption wavelengths of TiO_2-NTs, Cu_2O-NPs and Cu_2O-NPs/TiO_2-NTs-250s.

	Eg (eV)	λ_{abs} (nm)
TiO_2-NTs	3.2	387
Cu_2O-NPs	2.1 - 2.2*	563-590*
Cu_2O-NPs/TiO_2-NTs-250s	2.68	462

* According to literature [50, 51]

Table 2: L-H constants (kc and K) on Cu_2O-NPs/TiO_2-NTs-250s catalyst.

k_c: Kinetic constant of L-H ($mmol.m^{-3}.\ s.\ g_{TiO2}$)	K: Adsorption Constant of L-H ($m^3.\ mmol^{-1}$)
0.85	$2.2\ 10^{-3}$